

Cite this article as: Shi Chenxiao, Liu Yuanfu, Zhang Lele, et al. Microstructure and Oxidation Performance of TiC-MoSi₂ Reinforced Composite Coating Prepared by Plasma Transferred Arc Cladding[J]. Rare Metal Materials and Engineering, 2021, 50(08): 2686-2693.

ARTICLE

Microstructure and Oxidation Performance of TiC-MoSi₂ Reinforced Composite Coating Prepared by Plasma Transferred Arc Cladding

Shi Chenxiao¹, Liu Yuanfu^{1,2}, Zhang Lele¹, Chen Deqiang², Zhang Zheng¹, Liu Zhihong¹

¹ Materials Science and Engineering Research Center, School of Mechanical, Electronic and Control Engineering, Beijing Jiaotong University, Beijing 100044, China; ² National United Engineering Laboratory for Advanced Bearing Tribology, Henan University of Science & Technology, Luoyang 471003, China

Abstract: In order to improve the oxidation resistance and wear properties of AISI 304, a TiC-MoSi₂ complex phase enhanced composite coating was designed and in-situ prepared on AISI 304 substrate by plasma transferred arc (PTA) cladding technique. Microstructure of the composite coating before and after oxidation was analyzed. The hardness distribution of the coating was tested. The oxidation kinetics curves of the coating were measured and fitted. The oxidation mechanism of the coating was discussed. Results show that typical microstructure of the composite coating consists of TiC-MoSi₂ complex phases, primary TiC dendrites and γ -(Ni, Fe)/NiSi₂ eutectics. The TiC-MoSi₂ complex phases and TiC dendrites as reinforcing phases are uniformly distributed on the γ -(Ni, Fe)/NiSi₂ eutectic matrix. Due to the strengthening effect of the TiC-MoSi₂ complex phases and the binding and supporting action of the ultrafine γ -(Ni, Fe)/NiSi₂ eutectic matrix, the composite coating exhibits high and uniform hardness distribution, good strength and toughness. Thanks to its unique microstructure, the composite coating shows good oxidation resistance.

Key words: composite coating; microstructure; isothermal oxidation; synergistic strengthening

Intermetallic compound MoSi₂ is considered as one of the promising candidate for elevated temperature structural materials due to its high melting point (2030 °C), low density (6.24 g·cm⁻³), and good resistance to oxidation and hot corrosion^[1-6]. MoSi₂ is expected to be applied in aerospace and automotive fields, such as high temperature heat exchanger, aircraft turbine engine hot-section components and automotive turbochargers^[7-10]. However, the inherent shortcomings of monolithic MoSi₂ including insufficient high temperature strength and poor toughness at room temperature are major obstacles to the application of MoSi₂ as a structural material^[7]. In order to make MoSi₂ meet the requirements of structural materials, it is necessary to improve the fracture toughness at ambient temperature, as well as strength and creep resistance at elevated temperature. One of the most effective ways to solve above problems is introducing ductile reinforcements to form MoSi₂-based composites^[11-14]. The commonly used

toughing phases are some ductile metals like Al and transition metals, such as Nb, Mo and Ta, which are often dispersed in MoSi₂ matrix in the form of whiskers or fibers to improve the fracture toughness of MoSi₂. Jain et al^[13] fabricated hybrid laminated MoSi₂-based composites using Nb, Mo and Ta as reinforcing materials. They proved that these ductile metals can effectively improve the high temperature strength and creep resistance of MoSi₂-based composites. Lu et al^[14] prepared a 20vol% Nb particles reinforced MoSi₂ bulk composite and carried out a chevron-notched three-point flexure test. They found that the composite has excellent fracture strength and toughness; the rupture work of the composite is almost 5 times higher than that of the unreinforced MoSi₂. In addition, some ceramic particles or whiskers like SiC, TiC, Si₃N₄, ZrO₂ and Al₂O₃ are often used as brittle reinforcements of MoSi₂-based composites^[15-22]. Sun et al^[22] fabricated a 20vol% TiC whisker reinforced MoSi₂ matrix

Received date: August 22, 2020

Foundation item: Open Fund of National United Engineering Laboratory for Advanced Bearing Tribology, Henan University of Science and Technology (201904); Fundamental Research Funds for the Central Universities (2019JBZ106)

Corresponding author: Liu Yuanfu, Ph. D., Associate Professor, Materials Science and Engineering Research Center, Beijing Jiaotong University, Beijing 100044, P. R. China, Tel: 0086-10-51687034, E-mail: yfliu@bjtu.edu.cn

Copyright © 2021, Northwest Institute for Nonferrous Metal Research. Published by Science Press. All rights reserved.

composite. They reported that the room temperature flexural strength of the composite was 120% higher than that of pure MoSi_2 , and the room temperature fracture toughness was improved from $3.2 \text{ MPa}\cdot\text{m}^{1/2}$ to $5.2 \text{ MPa}\cdot\text{m}^{1/2}$. In fact, although many efforts have been made to improve the mechanical properties of MoSi_2 , it is still a huge challenge to make MoSi_2 a practical and feasible structural material. Despite MoSi_2 has inherent defects of poor mechanical properties, this does not prevent it from being used as a high quality antioxidant reinforcing phase for composites or composite coatings^[23-26].

TiC as a non-strict stoichiometric transition metal carbide has hybrid chemical bonds including covalent, ionic and metal bonds. Due to the extremely high covalent bond energy between Ti and C atoms, TiC has many advantages, such as high melting point (3067°C), high modulus of elasticity ($410\sim 450 \text{ GPa}$), high hardness ($28\ 000 \text{ MPa}$), and high temperature stability^[27]. Therefore, TiC is one of the most commonly used wear-resistant reinforcement phases for composites or composite coatings^[27-31]. It is proved that TiC is also an ideal strengthening and toughening phase for MoSi_2 -based composites^[32,33].

In this study, for improving the high temperature oxidation resistance and wear properties, a TiC- MoSi_2 complex phase enhanced γ -(Ni, Fe)/ Ni_2Si eutectic matrix composite coating was in-situ prepared on the AISI 304 substrate by PTA cladding technique. The microstructure of the composite coating before and after isothermal oxidation was comparatively analyzed. The oxidation behavior and anti-oxidation mechanism of the composite coating were studied.

1 Experiment

AISI 304 sheets with the size of $50 \text{ mm}\times 20 \text{ mm}\times 10 \text{ mm}$ were used as substrates. Surface of the substrates was polished with SiC sandpapers to remove the impurities, and then cleaned in acetone. Mixed powders of Ni, Mo, Si, Ti and C with composition of Ni-27.2Mo-15.8Si-3.4C-13.6Ti (wt%) was used as raw material for in-situ synthesizing the MoSi_2 -TiC+TiC/ γ -(Ni, Fe)/ Ni_2Si composite coating. Average particle size of the mixed powders was about $70 \mu\text{m}$ and the purity was about 99.99%. Before PTA cladding, the powders were mixed in a planetary ball mill for 10 h and dried in a blast drying oven at 150°C for 6 h.

Single-track PTA cladding experiment was performed on a PTA cladding system to prepare the composite coating. The PTA cladding system was equipped with a patented PTA torch^[34] and a four-axis computer numerically controlled (CNC) machine. Operating principle of the PTA torch was introduced in our previous work in detail^[35]. Parameters of the PTA cladding process were optimized by preliminary exploration experiments. The optimized parameters are listed as follows: operating voltage 35 V , operating current 105 A , scanning speed $2 \text{ mm}\cdot\text{s}^{-1}$, powder feeding speed $25\sim 30 \text{ g}\cdot\text{min}^{-1}$, working gas (argon) flux $80 \text{ L}\cdot\text{h}^{-1}$, and shielding gas (argon) flux $120 \text{ L}\cdot\text{h}^{-1}$.

Metallographic samples were prepared using standard mechanical polishing procedures and chemically etched in

H_2O -7vol% HF-43vol% HNO_3 water solution for approximately 25~35 s. Microstructure and phase composition of the composite coating were characterized by optical microscope (OM, MDS), scanning electron microscope (SEM, Quanta 200 FEG) and X-ray diffraction (XRD, Rigaku D/max 2200) with Cu $\text{K}\alpha$ radiation. Energy dispersive spectroscopy (EDS, LinkISIS) was used to analyze the chemical composition of the constituent phases of the coating.

Microhardness distribution along the depth direction of the coating was measured by Vickers microhardness tester (HV, MH-5L) with a test load of 0.5 kg and a load-dwell time of 12 s.

Isothermal oxidation experiments in atmospheric environment were carried out by a box-type resistance furnace. The experimental temperature of isothermal oxidation was 800, 1000 and 1200°C . Top surface of the composite coating was firstly ground to a smooth plane by mechanical milling. Subsequently, the entire coating was separated from the AISI 304 substrate by electrical discharge machining and cut into rectangular sheet. Size of the rectangular sheet samples was $5 \text{ mm}\times 5 \text{ mm}\times 1.2 \text{ mm}$. All the surfaces of the samples were polished with 800# grit abrasive papers and cleaned with alcohol. Each surface area of the samples was measured by Vernier caliper with a precision of 0.01 mm. The total surface area of each sample was obtained by adding each surface area together. Each sample was weighed by an electronic balance with a precision of 0.1 mg before (m_0) and after (m_1) oxidation experiment. The mass gain per unit area S (Δw) of each sample was calculated using the following equation.

$$\Delta w = \frac{m_1 - m_0}{S} \quad (1)$$

2 Results and Discussion

2.1 Microstructure of the composite coating

Fig.1 shows the XRD pattern of the PTA cladding composite coating. The composite coating consists mainly of MoSi_2 , TiC, γ -(Ni, Fe) and a small amount of Ni_2Si . During the PTA cladding process, a small amount of AISI 304 substrate (mainly containing Fe) was unavoidably melted into the molten pool. With rapid solidification of the molten pool, these iron atoms were dissolved into the γ -Ni as substitute

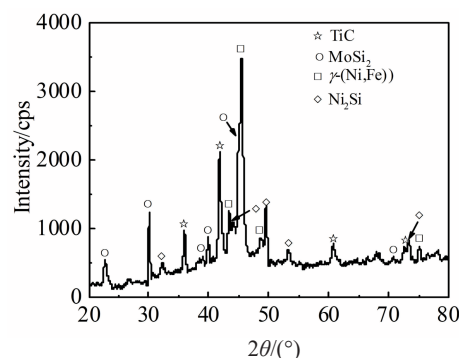


Fig.1 XRD pattern of the PTA cladding composite coating

atoms, resulting in the formation of γ -(Ni, Fe) solid solutions.

Fig. 2 shows the cross-section microstructure of the PTA cladding composite coating. There is a fusion line with a width of about 40 μm between the coating and the AISI 304 substrate. Similar to the laser cladding process^[36], the PTA cladding molten pool mainly dissipates heat through the conduction of the substrate, so the temperature gradient at the bottom of the molten pool is the largest. Meanwhile, since the bottom of the molten pool is the initial solid/liquid interface, the nucleation energy required for the melt at the bottom of the molten pool is the minimal. Therefore, the melt first nucleates at the bottom of the molten pool, and advances towards the inside of the molten pool with an approximately planar solid/liquid interface, gradually forming the fusion line. By means of the fusion line, a complete metallurgical bond is formed between the PTA cladding coating and the substrate.

Typical microstructure of the composite coating was observed in detail using SEM at different magnifications. As shown in Fig. 3a, typical microstructure of the composite coating consists of dark gray fine particles, dark gray dendrites, white gray polygonal blocks and lamellar eutectics. Volume fraction of the eutectics is about 22vol%, and the remaining constituent phases are about 78vol%. Fig.3b clearly shows the microstructural features. The dark gray fine particles with an average particle size of about 4 μm are dispersed on the white gray polygonal blocks and the lamellar eutectics. The lamellar eutectics consist of two phases, including white strips and dark gray granular particles or dark gray strips. The microstructure in which dark gray fine particles are scattered in the white gray polygonal blocks shown in Fig.3b is called complex phase.

EDS analysis results indicate that the content of Mo and Si in the white gray polygonal block phases is 31.36at% and 68.64at%, respectively. Combined with XRD analysis results (Fig. 2), the white gray polygonal block phases should be identified as MoSi_2 . The content of C, Ti and Mo in the dark gray dendrites or particles is 37.67at%, 59.14at%, and 3.19at%, respectively. The dark gray particles and dendrites should be TiC with a small amount of Mo atoms dissolved. The content of Ni, Si, Fe and Cr in the lamellar eutectics is

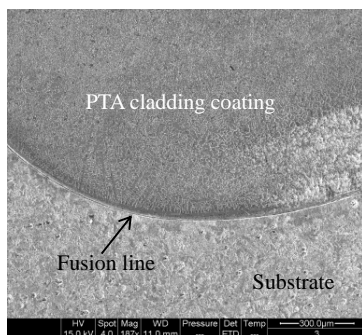


Fig.2 SEM image of cross-section microstructure of the PTA cladding composite coating

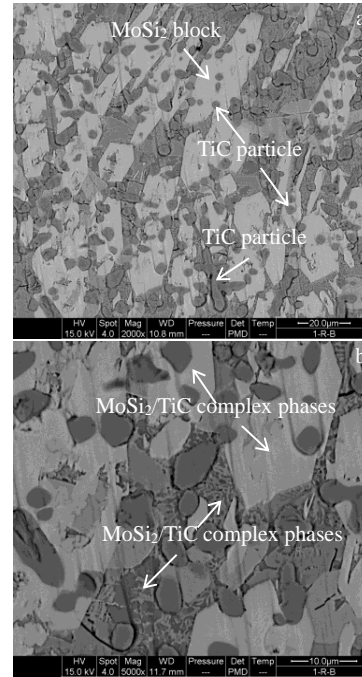


Fig.3 SEM image of distribution of the constituent phases of the coating (a) and microstructure details of the complex phases and the lamellar eutectics (b)

63.38at% , 19.35at% , 15.73at% and 1.55at% , respectively. Combined with XRD analysis results, the eutectics can be identified as $\text{Ni}_2\text{Si}/\gamma$ -(Ni, Fe); the white strips are γ -(Ni, Fe), and the dark-grey granular particles or dark-grey strips are Ni_2Si silicide.

According to above analysis, it is known that the main constituent phases of the composite coating are primary TiC dendrites, TiC-MiSi₂ complex phases and (Ni, Fe)/Ni₂Si eutectics. The primary TiC dendrites and TiC-MiSi₂ complex phases as the reinforcing phases are uniformly dispersed on the (Ni, Fe)/Ni₂Si binary eutectic matrix.

The formation process of the TiC-MiSi₂ complex phases is as follows. For the Ni, Mo, Si, Ti, C system, TiC has the highest melting point and the most negative Gibbs free energy (-130.348 kJ·mol⁻¹ at 3400 K), so TiC first precipitates from the PTA melting pool in the form of fine particles and dendrites. Subsequently, the Mo and Si atoms with the fine TiC particles as heterogeneous nuclei are aggregated and nucleated around the TiC particles, and grow into TiC-MoSi₂ complex phases. Since the TiC-MoSi₂ complex phase is in-situ synthesized, the interface compatibility between TiC and MoSi₂ is good, which ensures that the dispersed micron-scale TiC particles can play an effective dispersion strengthening role in the TiC-MoSi₂ complex phase. The rapid solidification of the PTA melting pool inhibits the growth of the TiC-MoSi₂ complex phases, resulting in relatively fine grains of the TiC-MoSi₂ complex phases. Therefore, the TiC-MoSi₂ complex phases also obtain fine grain strengthening. It is no doubt that the strength and toughness of the TiC-MoSi₂ complex phases

can be effectively improved by fine grain strengthening and dispersion strengthening, and the inherent defects of the monolithic MoSi_2 material such as insufficient high temperature strength and poor toughness can be effectively overcome.

2.2 Microhardness of the composite coating

Fig. 4 shows the microhardness distribution curve of the composite coating along the cross-sectional depth direction. Average microhardness value of the composite coating is about 8750 MPa, which is approximately 3.6 times higher than that of the AISI 304 substrate. From the surface to a depth of about 900 μm , the microhardness values of the coating fluctuate slightly around 9400 MPa. In this region, the TiC primary dendrites and the TiC- MoSi_2 complex phases with high volume fraction are dispersed on the γ -(Ni, Fe)/ NiSi_2 eutectic matrix. Within the depth of 900 μm to 1500 μm from the coating surface, microhardness values gradually decrease from 8300 MPa to 2400 MPa (the hardness level of AISI 304 substrate). This region corresponds to the bonding zone, where the coating is diluted by the AISI 304 substrate, resulting in a low content of TiC and MoSi_2 hardness phases, so the hardness of this region is relatively low.

As shown in the inset in Fig.4, under the test condition of a load of 0.5 kg and a load holding time of 12 s, the composite coating does not crack near the four corners, where stress concentration exists, of diamond indentation. Above result indicates that the composite coating has both high hardness and good strength and toughness. Obviously, the good mechanical properties of the composite coating are not only attributed to the strengthening of the TiC- MoSi_2 complex phases with high volume fraction and high hardness, but also to the bonding and supporting effect of the ultrafine γ -(Ni, Fe)/ NiSi_2 eutectic matrix with good toughness.

2.3 Oxidation resistance

In order to more intuitively show the difference in high temperature oxidation resistance between the PTA cladding coating and the AISI 304 reference sample, the relative oxidation resistance was used. As shown in Fig.5, the relative

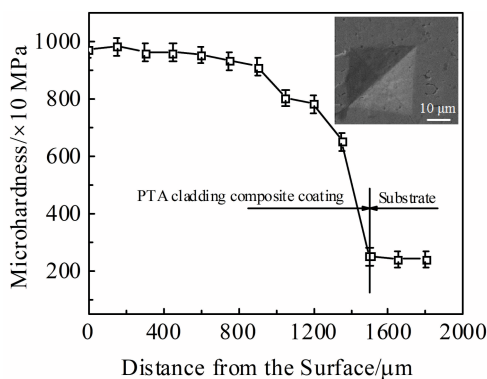


Fig.4 Microhardness distribution curve of the PTA cladding composite coating (inset is SEM image showing the morphology of the composite coating around the diamond indentation)

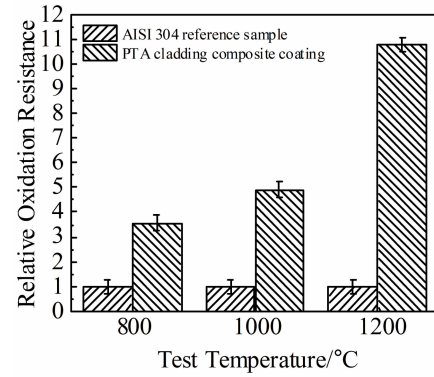


Fig.5 Relationship between relative oxidation resistance and oxidation temperature of the PTA cladding coating

oxidation resistance of PTA cladding coating increases correspondingly with the increase of the oxidation temperature, which means that the PTA cladding coating has good high temperature oxidation resistance compared with the AISI 304 reference sample, and the higher the oxidation temperature, the more obvious the advantage of the PTA cladding coating.

Fig.6 shows the fitted isothermal oxidation kinetic curves of the PTA cladding coatings and the AISI 304 reference samples. It can be known that the oxidation kinetics curves of the PTA cladding coating under the test conditions of isothermal oxidation at 800, 1000, and 1200 $^{\circ}\text{C}$ for 50 h roughly conform to the logarithm law. The oxidation kinetics curves of the AISI 304 reference sample after isothermal oxidation at 800 and 1000 $^{\circ}\text{C}$ for 50 h are approximately consistent with the parabolic law. However, when AISI 304 is oxidized isothermally at 1200 $^{\circ}\text{C}$, its oxidation kinetics curve approximates to the linear law.

2.4 Oxidation mechanism of the AISI 304

Fig.7 is the XRD pattern of the AISI 304 reference sample after isothermal oxidation at 1000 $^{\circ}\text{C}$ for 50 h. As shown in Fig.7, diffraction peaks of Fe_2O_3 , Cr_2O_3 and NiO are identified

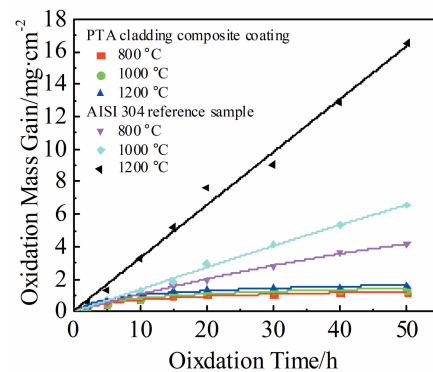


Fig.6 Fitted isothermal oxidation kinetics curves of the PTA cladding composite coating and the AISI 304 reference sample

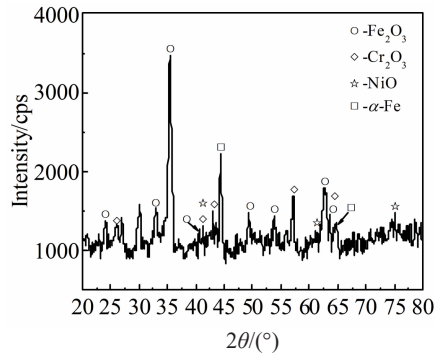


Fig.7 XRD pattern of the AISI 304 reference specimen after isothermal oxidation at 1000 °C for 50 h

in the XRD pattern, which means that an oxide film consisting of Cr_2O_3 , Fe_2O_3 and NiO forms on the surface of AISI 304.

Fig.8 shows the surface morphologies of the oxide film. As shown in Fig. 8, the oxide film is relatively dense and continuous as a whole, except for a few micro-cracks and micro-peeling pits in local areas (Fig.8b). During isothermal oxidation process of AISI 304, growth stress and thermal stress act on the oxide film together, resulting in a small amount of micro-cracks and micro-peeling pits in the local area of the oxide film. Due to the small number and shallow depth of these micro-cracks and micro-peeling pits, these micro-cracks and micro-peeling pits do not become short-circuit channels for ion diffusion. Therefore, the AISI 304 reference samples still have good antioxidant protection effect, and their oxidation kinetics curves are still approximately consistent with the parabolic law, as shown in

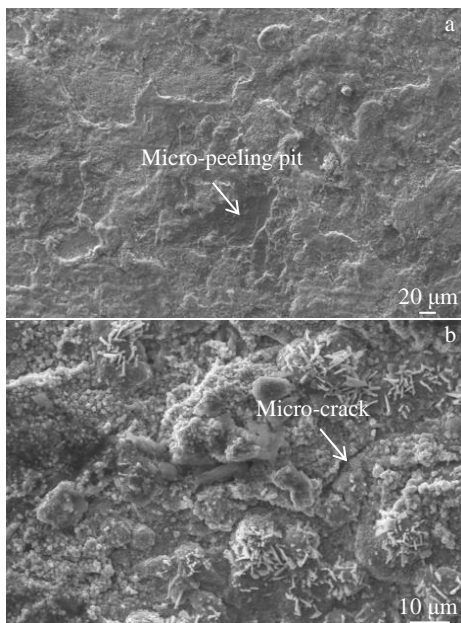


Fig.8 SEM images of surface morphology (a) and surface microstructure details of the oxide film (b)

Fig. 6. However, when the oxidation temperature reaches 1200 °C, most of the oxide film on AISI 304 peels off, so its oxidation kinetic curve conforms to the linear law.

2.5 Oxidation mechanism of the PTA cladding coating

Fig.9 is the XRD pattern of the PTA cladding composite coating after isothermal oxidation at 1000 °C for 50 h. Diffraction peaks of TiO_2 , SiO_2 and NiO are identified, which means that the surface layer of the PTA cladding composite coating is oxidized into an oxide film composed of TiO_2 , SiO_2 and NiO .

Fig.10 shows the surface morphologies of the oxide film. As shown in Fig.10a, the oxide film consists of hemispherical particle clusters, submicron particles and planar matrix. The submicron particles and the hemispherical particle clusters are uniformly dispersed on the planar matrix. The hemispherical particle clusters present two different morphologies. One is composed of rectangular particles and a small number of nanoscale spherical particles, as shown in Fig.10b. The other consists entirely of nanoscale spherical particles, as shown in Fig.10c.

EDS analysis results indicate that chemical composition of the particle clusters shown in Fig.10b is 22.69Ni-19.70Ti-55.69O-0.21Si-1.72Pt (at%). In order to improve the electrical conductivity of the oxidized samples to obtain clear SEM images, a Pt-Au alloy thin film was deposited on the surface of the samples by physical vapor deposition (PVD), so the peak of Pt appears in the EDS spectrum. Combined with XRD analysis results, it can be inferred that the particle clusters shown in Fig.10b are composed of NiO and TiO_2 , among which the rectangular blocks are NiO and the nanoscale spherical particles are TiO_2 . The content of Ti and O in the particle clusters shown in Fig.10c is 36.60at% and 59.56at%, respectively. Combined with XRD analysis results, it can be concluded that the particle clusters consist entirely of TiO_2 . The submicron particles shown in Fig.10c mainly contain O, Ni and a small amount of Ti. Combined with XRD analysis results, it can be inferred that these submicron particles are NiO . The planar matrix shown in Fig.10c mainly contains Ni, Ti, Si and O. Combined with XRD analysis results, it can be inferred that the planar matrix is composed of NiO , SiO_2 and a small amount of TiO_2 .

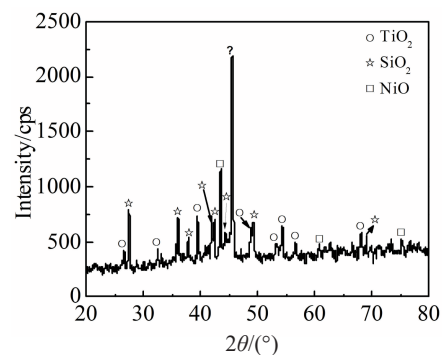


Fig.9 XRD pattern of the PTA cladding composite coating after isothermal oxidation at 1000 °C for 50 h

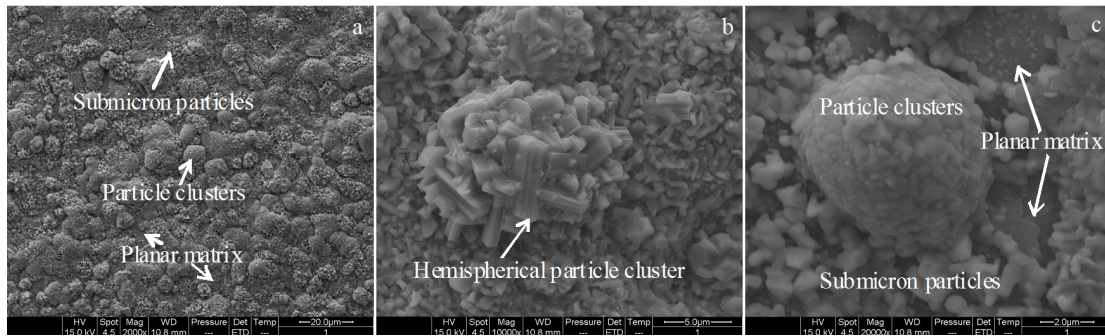


Fig.10 SEM images of surface morphology of oxide film (a), microstructure of the particle cluster composed of rectangular particles and nanoscale spherical particles (b), and particle cluster composed entirely of nanoscale spherical particles (c)

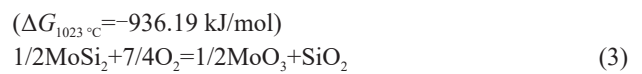
It can be concluded that the surface layer of the PTA cladding composite coating is oxidized into a composite oxide film composed of NiO, SiO₂ and TiO₂ after 50 h of isothermal oxidation at 1000 °C. Obviously, it is the effective blocking effect of SiO₂ and TiO₂ on ion diffusion that makes the composite oxide film have excellent oxidation resistance.

Fig. 11 shows the cross-sectional SEM image and the EDS linear scanning profiles of the composite oxide film. As shown in Fig. 11a, the average thickness of the composite oxide film is about 30 μm. There are no defects such as micropores and micro-cracks inside the composite oxide film. The oxide film is well bonded to the PTA cladding coating. As shown in Fig. 11b, the oxygen content in the oxide film is high and stable, while that in the PTA coating is close to zero,

which indicates that the oxide film effectively blocks the diffusion of oxygen ions. From the surface of the oxide film to the depth of 15 μm, the content of Si and Ni is higher, while the content of Ti is lower. Combined with the XRD analysis results (Fig. 9), it can be inferred that within above range, the oxide film is mainly composed of SiO₂, NiO and a small amount of TiO₂. Within the range of 15 μm to 30 μm from the surface of the oxide film, the content of Ni and Si decreases sharply (close to zero), while the content of Ti increases rapidly, which indicates that the main constituent phase of the oxide film in this region is TiO₂.

In order to investigate the detailed distribution of O, Ti, Si and Ni on the cross section of the oxide film, the EDS elemental map was adopted. As shown in Fig. 12, the outer layer of the oxide film mainly contains O, Ni and Si, while the inner layer mainly contains O and Ti, which is consistent with the EDS linear scan results (Fig. 11b). Combining the results of EDS linear scanning and EDS elemental maps, it can be concluded that the composite oxide film obviously has a double-layer structure; the outer layer mainly contains SiO₂ and NiO, and the inner layer mainly contains TiO₂.

Fig. 13 is a schematic diagram of the microstructure evolution of the PTA cladding composite coating during high temperature oxidation process. During oxidation process, the constituent phases of the PTA coating including TiC, MoSi₂ and γ-(Ni, Fe) undergo the following oxidation reactions, as shown in Eq.(2~4), respectively.



Although the standard Gibbs free energy (ΔG) required to form TiO₂, SiO₂, and NiO is significantly different, because of the high oxygen partial pressure in the initial stage of oxidation process, the oxidation reaction shown in Eq. (2~4) can proceed smoothly. As a result, a composite oxide film mainly composed of SiO₂, NiO and a small amount of TiO₂ is formed in the initial stage of oxidation process. Because the

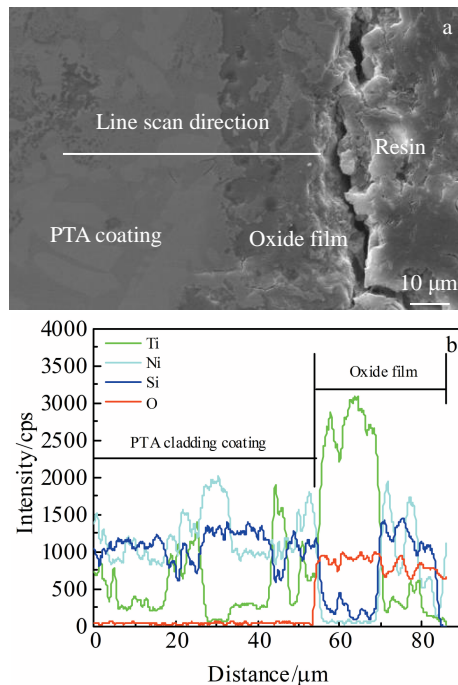


Fig.11 Cross-sectional SEM image (a) and EDS linear scanning profiles (b) of the composite oxide film (isothermal oxidation at 1000 °C for 50 h)

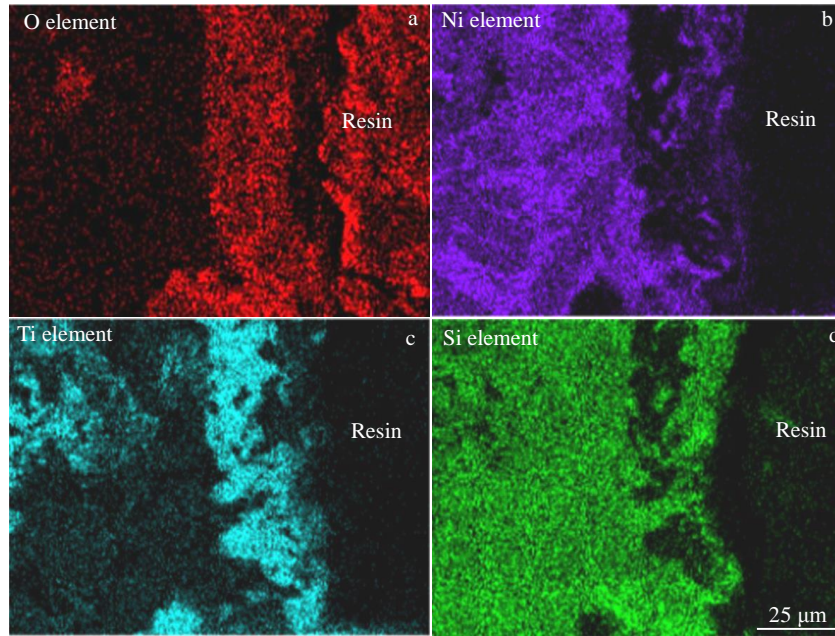


Fig.12 EDS maps in the cross section of oxide film shown in Fig.11a: (a) O, (b) Ni, (c) Ti, and (d) Si

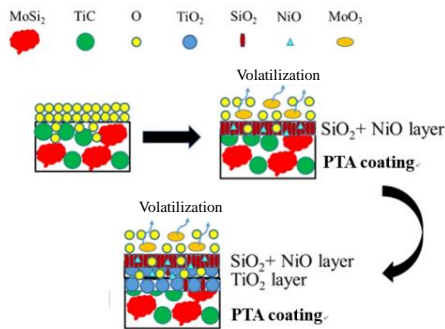


Fig.13 Schematic diagram of the microstructure evolution of the PTA cladding coating during isothermal oxidation process

content of TiC in the PTA cladding composite coating is significantly less than that of MoSi₂ and γ -(Ni, Fe), the content of TiO₂ in the initially formed oxide film is relatively low. When the PTA cladding coating sample is completely covered by the oxide film, the oxidation reaction can continue only when the oxygen anions and metal cations successfully pass through the oxide film by solid state diffusion. Due to the relatively large radius of oxygen anions, it is difficult for the oxygen anions to pass through the oxide film, resulting in oxygen anion deficiency in the area between the oxide film and the unoxidized PTA cladding coating. In the above oxygen anion deficient environment, according to the thermodynamic principle, the reaction shown in Eq. (2) proceeds preferentially, so the main constituent phase of the inner layer of the oxide film is TiO₂. The formation of a double-layer dense composite oxide film further increases the difficulty of ion diffusion. Therefore, the subsequent oxidation reactions proceed at a steady and slow rate, exhibiting a

logarithmic oxidation kinetic curve shown in Fig.6.

3 Conclusions

1) A TiC-MoSi₂+TiC/ γ -(Ni, Fe)/NiSi₂ composite coating can be in-situ prepared on the surface of AISI 304 by PTA cladding process using the powder blend of Ni, Mo, Si, Ti and C as raw materials.

2) The composite coating consists of primary TiC dendrites, TiC-MoSi₂ complex phases and γ -(Ni, Fe)/NiSi₂ binary eutectics. TiC and TiC-MoSi₂ as reinforcement phases are uniformly scattered on the γ -(Ni, Fe)/NiSi₂ eutectic matrix.

3) Due to the strengthening of the TiC-MoSi₂ complex phases, and the bonding and supporting of the ultrafine γ -(Ni, Fe)/NiSi₂ matrix, the composite coating exhibits high and uniform hardness distribution, as well as good strength and toughness.

4) After isothermal oxidation, a dense and continuous composite oxide film with a double layer structure is formed on the surface of the PTA cladding coating. Outer layer of the oxide film is mainly composed of SiO₂ and NiO, and inner layer of the oxide film mainly contains TiO₂. The composite oxide film exhibits excellent high temperature oxidation resistance.

References

- 1 Petrovic J J, Vasudevan A K. *Materials Science Engineering A* [J], 1999, 261: 1
- 2 Yang J M, Kai W, Jeng S M. *Scripta Metallurgica*[J], 1989, 23: 1953
- 3 Wade R K, Petrovic J J. *Journal of the American Ceramic Society*[J], 1992, 75: 3160
- 4 Jayashankar S, Kaufman M J. *Scripta Metallurgica et Materialia*

- [J], 1992, 26: 1245
- 5 Schlichting J. *Ceramurgia International*[J], 1978, 4: 162
 - 6 Meschter P J, Schwartz D S. *Journal of the Minerals Metals & Materials Society*[J], 1989, 41: 52
 - 7 Vasudévan A K, Petrovic J J. *Materials Science Engineering A* [J], 1992, 155: 1
 - 8 Petrovic J J. *Intermetallics*[J], 2000, 8: 1175
 - 9 Sastry S M L, Suryanarayanan R, Jerina K L. *Materials Science Engineering A*[J], 1995, 192-193: 811
 - 10 Costae Silva A, Kaufman M J. *Intermetallics*[J], 1997, 5: 1
 - 11 Tao X, Liu J C, Xu X J et al. *Journal Alloys Compounds*[J], 2016, 684: 488
 - 12 Sánchez-González E, Borrero-López O, Guiberteau F et al. *Journal of the European Ceramic Society*[J], 2016, 36: 3091
 - 13 Jain M K, Das J, Subrahmanyam S J et al. *International Journal of Refractory Metals & Hard Materials*[J], 2017, 66: 258
 - 14 Lu T C, Evans A G, Hecht R J et al. *Acta Metallurgica et Materialia*[J], 1991, 39: 1853
 - 15 He Z B, Li H J, Shi X H et al. *Progress in Natural Science: Materials International*[J], 2014, 24: 247
 - 16 Huang Y, Lin J, Zhang H A. *Ceramics International*[J], 2015, 41: 13 903
 - 17 Wang L, Fu Q G, Zhao F L. *Intermetallics*[J], 2018, 94: 106
 - 18 Fu Q G, Zhang J P, Zhang Z Z et al. *Transactions of Nonferrous Metals Society of China*[J], 2013, 23: 2123
 - 19 Ignat S, Sallamand P, Nichici A et al. *Surface & Coatings Technology*[J], 2003, 172: 233
 - 20 Cao L Y, Bai Z, Huang J F et al. *Journal Alloys Compounds*[J], 2017, 70: 345
 - 21 Petrovic J J, Bhattacharya A K, Honnell R E et al. *Materials Science Engineering A* [J], 1992, 155: 259
 - 22 Sun L, Pan J S. *Materials Letters*[J], 2001, 51: 270
 - 23 Yang K M, Wang J X, Yang S Y et al. *Surface & Coatings Technology* [J], 2018, 354: 324
 - 24 Bezzi F, Burgio F, Fabbri P et al. *Journal of the European Ceramic Society* [J], 2019, 39: 79
 - 25 Carabat A L, Meijerink M J, Brouwer J C et al. *Journal of the European Ceramic Society* [J], 2018, 38: 2728
 - 26 Liang J, Liu X B, Ke J et al. *Surface & Coatings Technology*[J], 2019, 372: 56
 - 27 Liu S Y, Shin Y C. *Materials Design*[J], 2017, 136: 185
 - 28 Ding H M, Wang X L, Liu Q et al. *Materials Design*[J], 2017, 135: 232
 - 29 Gorji M R, Edtmaier C, Sanjabi S. *Materials Design*[J], 125: 167
 - 30 Deng J X, Liu L L, Yang X F et al. *Materials Design*[J], 2007, 28: 757
 - 31 Zhou Z Y, Liu X B, Zhuang S G et al. *Applied Surface Science* [J], 2019, 481: 209
 - 32 Sun L, Pan J S. *Journal of the European Ceramic Society*[J], 2002, 22: 791
 - 33 Feng Z C, Liu Y F, Li Y et al. *Tribology International*[J], 2019, 129: 82
 - 34 Liu Y F, Peng Y B, Zhang Y X et al. *Chinese Patent*, ZL201410392015.7[P], 2014
 - 35 Liu Y F, Feng Z C, Pu F et al. *Surface & Coatings Technology* [J], 2018, 345: 61
 - 36 Lu X L, Liu X B, Yu P C et al. *Tribology International*[J], 2016, 101: 356

转移等离子弧熔敷 TiC-MoSi₂增强复合涂层显微组织及抗氧化性

石晨晓¹, 刘元富^{1,2}, 张乐乐¹, 陈德强², 张政¹, 刘志宏¹

(1. 北京交通大学机械与电子控制工程学院材料科学与工程研究中心, 北京 100044)

(2. 河南科技大学 高端轴承摩擦学技术与应用国家地方联合工程实验室, 河南 洛阳 471003)

摘要: 为了提高 AISI 304 不锈钢的高温抗氧化性及耐磨性, 利用转移等离子弧熔敷技术在 AISI 304 基材表面制备了 TiC-MoSi₂ 复合相增强复合涂层。对比分析了氧化前后复合涂层的显微组织, 测试了复合涂层的显微硬度分布, 测试并拟合了复合涂层的氧化动力学曲线, 探讨了复合涂层的氧化机理。结果表明: 复合涂层典型显微组织由 TiC-MoSi₂ 复合相、初生 TiC 枝晶和 γ -(Ni,Fe)/NiSi₂ 共晶构成, TiC-MoSi₂ 复合相和初生 TiC 枝晶作为复合涂层的增强相均匀分布在 γ -(Ni,Fe)/NiSi₂ 共晶基体上。由于 TiC-MoSi₂ 复合相的增强作用以及超细 γ -(Ni,Fe)/NiSi₂ 共晶基体的粘结和支撑作用, 复合涂层具有高且均匀的硬度分布、良好的强度和韧性。得益于独特的显微组织, 复合涂层表现出良好的高温抗氧化性。

关键词: 复合涂层; 显微组织; 等温氧化; 协同增强

作者简介: 石晨晓, 男, 1997年生, 硕士, 北京交通大学机械与电子控制工程学院材料科学与工程研究中心, 北京 100044, 电话: 010-51687034, E-mail: 16121353@bjtu.edu.cn